blood advances

American Society of Hematology
2021 L Street NW, Suite 900,
Washington, DC 20036
Phone: 202-776-0544 | Fax 202-776-0545
bloodadvances@hematology.org

Lysosomal Degradation Targets Mutant Calreticulin and the Thrombopoietin Receptor in Myeloproliferative Neoplasms

Tracking no: ADV-2023-011432R1

Amanpreet Kaur (University of Michigan Medical School, United States) Arunkumar Venkatesan (Department of Ophthalmology & Visual Sciences, Upstate Medical University, Syracuse, NY, USA, United States) Malathi Kandarpa (University of Michigan, United States) Moshe Talpaz (University of Michigan, United States) Malini Raghavan (University of Michigan Medical School, United States)

Abstract:
Somatic mutants of calreticulin (CRT) drive myeloproliferative neoplasms (MPNs) via binding to the thrombopoietin receptor (MPL) and aberrant activation of the JAK/STAT pathway. Compared with healthy donors, platelets from MPN patients with CRT mutations display low cell surface MPL. Additionally, co-expression of MPL with an MPN-linked CRT mutant (CRTDel52) reduces cell surface MPL, suggesting that CRTDel52 may induce MPL degradation. We show that lysosomal degradation is relevant to the turnover of CRTDel52 and MPL. Furthermore, CRTDel52 increases the lysosomal localization and degradation of MPL. Mammalian target of rapamycin (mTOR) inhibitors reduce cellular CRTDel52, MPL and secreted CRTDel52 levels, and impair CRTDel52-mediated cell proliferation. mTOR inhibition also reduces colony formation and differentiation of CD34+ cells from MPN patients but not healthy donors. Together, these findings indicate low surface MPL as a biomarker of mutant CRT-mediated MPN and induced degradation of CRTDel52 and MPL as an avenue for therapeutic intervention.

Conflict of interest: COI declared - see note

COI notes: Dr. Moshe Talpaz serves as advisory board member for Sierra Oncology, Bristol Myers Squibb, Sumitomo and GlaxoSmithKline/Pfizer and has received research support from Bristol Myers Squibb, Novartis, Sumitomo and Morphosys.

Preprint server: Yes; bioRxiv 10.1101/2023.07.12.548605

Author contributions and disclosures: AK and AV designed and performed experiments, analyzed data, wrote the original draft and edited the manuscript. MK collected patient blood and bone marrow samples, purified platelets and edited the manuscript. MT is the director of MPN repository at the University of Michigan, helped with study design and read the manuscript. MR designed and supervised the study, obtained funding, analyzed data, and wrote, and edited the manuscript.

Non-author contributions and disclosures: No;

Agreement to Share Publication-Related Data and Data Sharing Statement: Public Deposit and emails to the corresponding author

Clinical trial registration information (if any):

Lysosomal Degradation Targets Mutant Calreticulin and the Thrombopoietin Receptor in Myeloproliferative Neoplasms

Amanpreet Kaur[1], Arunkumar Venkatesan[1, 2], Malathi Kandarpa[3], Moshe Talpaz[3] and Malini Raghavan[1*]

[1]Department of Microbiology and Immunology, University of Michigan Medical School, Ann Arbor, MI, USA, 48109
[2]Current Address: Department of Ophthalmology & Visual Sciences, Upstate Medical University, Syracuse, NY, USA, 13202
[3]Department of Internal Medicine, Division of Hematology/Oncology, University of Michigan Rogel Cancer Center, Ann Arbor, MI, USA, 48109

*Correspondence to Malini Raghavan, PhD: malinir@umich.edu

Short title: Degradation of Mutant Calreticulin and MPL in MPN

Data Sharing

Public Deposit and emails to the corresponding author

Key Points

- **Lysosomal degradation regulates cellular CRT_{Del52} and MPL levels.**
- **mTOR inhibitors reduce CRT_{Del52} and MPL levels and reduce CRT_{Del52}-induced cell proliferation.**

Abstract

Somatic mutants of calreticulin (CRT) drive myeloproliferative neoplasms (MPNs) via binding to the thrombopoietin receptor (MPL) and aberrant activation of the JAK/STAT pathway. Compared with healthy donors, platelets from MPN patients with CRT mutations display low cell surface MPL. Additionally, co-expression of MPL with an MPN-linked CRT mutant (CRT_{Del52}) reduces cell surface MPL, suggesting that CRT_{Del52} may induce MPL degradation. We show that lysosomal degradation is relevant to the turnover of CRT_{Del52} and MPL. Furthermore, CRT_{Del52} increases the lysosomal localization and degradation of MPL. Mammalian target of rapamycin (mTOR) inhibitors reduce cellular CRT_{Del52}, MPL and secreted CRT_{Del52} levels, and impair CRT_{Del52}-mediated cell proliferation. mTOR inhibition also reduces colony formation and differentiation of $CD34^+$ cells from MPN patients but not healthy donors. Together, these findings indicate low surface MPL as a biomarker of mutant CRT-mediated MPN and induced degradation of CRT_{Del52} and MPL as an avenue for therapeutic intervention.

Keywords

Myeloproliferative Neoplasms, calreticulin, MPL, thrombopoietin receptor, lysosomal degradation, rapamycin, everolimus, mTOR inhibitors

Introduction

Essential thrombocythemia (ET), polycythemia vera (PV), and myelofibrosis (MF) are myeloproliferative neoplasms (MPNs) that include hyperproliferation of myeloid lineage blood cells [1,2]. Somatic mutations of the calreticulin (CRT) gene are found in 20-35 % of ET and MF patients [3,4]. Most of these mutations are +1 bp frame shift mutations in the exon 9 that encodes the carboxy domain of CRT. The type 1 mutation, which involves a 52 bp deletion (Del52), and the type 2 mutation, which involves a 5 bp insertion (Ins5), account for 45 to 53% and 32 to 41% of CRT mutations in MPNs, respectively [3,4]. MPN-linked mutant CRT proteins are characterized by enrichment of basic amino acids in the carboxy domain in contrast to acidic amino acids present in wild-type CRT [3,4]. The MPN CRT mutants also lack the KDEL motif at the carboxy-terminal end which is responsible for endoplasmic reticulum (ER) localization of wild-type protein. Loss of the KDEL sequence affects ER retention [3-5] and induces secretion of MPN-linked CRT mutants [6-9].

The pathogenic effects of mutant CRT proteins in MPNs are attributed in part to their ability to induce ligand-independent constitutive activation of JAK/STAT signaling via the cell surface receptor, MPL (also called the thrombopoietin receptor (TPOR)), which is a known glycoprotein substrate of CRT [10-14]. While the interaction between MPL and wild-type CRT is transient, mutant CRT proteins form stable complexes with MPL via both the glycan-binding site [5,14-16] and the novel C-terminal domain [15,17,18]. The mutant CRT and MPL complexes co-traffic to the cell surface [5]. MPL is expressed on the surface of hematopoietic cells and regulates the differentiation of megakaryocytes and production of platelets as well as self-renewal of hematopoietic stem cells (HSCs) [19-21]. Expression of MPN-linked mutant CRT proteins and the resultant activation of MPL signaling promotes proliferation of megakaryocytes and excessive production of platelets [10,11,13,22-24].

The physiological activation of MPL signaling by TPO is tightly regulated via a coordination between the synthesis and release of TPO, and its removal from blood circulation [25]. Binding of TPO to MPL and the resultant activation of receptor signaling is followed by internalization and degradation of the receptor-ligand complex which removes excess TPO from circulation [26-29]. However, little is known about the downstream effects of MPL signaling activated by the binding of MPN-linked mutant CRT proteins. In this study, we measured the relative levels of MPL protein on platelets purified from MPN patients and healthy donors and found a significant reduction in MPL levels in MPN patient platelets. We used model cell lines co-expressing human MPL and mutant CRT proteins to explore pathways involved in the regulation of surface MPL and mutant CRT levels. Our findings also indicate that induced degradation of mutant CRT and MPL can be used therapeutically to compromise the cell-transforming effects of mutant CRT.

Methods

Study Approval

Blood samples were collected after obtaining written informed consent from donors and MPN patients following protocols approved by the University of Michigan Institutional Review Board. MPN patient blood samples were collected from the Myeloproliferative diseases repository (study ID: HUM0006778). Healthy donor blood samples were obtained from the University of Michigan Platelet Physiology and Pharmacology Core repository (study ID: HUM00107120) and from participants of another research study (study ID: HUM00071750).

DNA Constructs

The pMSCV and pcDNA3.1/Zeo(-) constructs used for expression of untagged CRT_{WT} and CRT_{Del52} in mammalian cells have been described earlier [17]. A human MPL construct (accession number BC153092) was purchased from DNASU and subcloned into pMSCV-neomycin vector at EcoRI and XhoI sites, and into pcDNA-COX2-54 vector by LIC as described earlier[17]. All primers used are specified in Supplemental Table 1.

Proliferation assays and colony forming unit assays

Proliferation assays of Ba/F3-MPL cells were performed with or without treatment with everolimus or rapamycin for five days. For CFU assays, $CD34^+$ cells isolated from bone marrow samples from MPN patients (Supplemental Table 3) or leukopaks from healthy donors were used. Detailed protocols are given in supplemental information.

Blood samples were collected after obtaining written informed consent from donors and Myeloproliferative Neoplasm patients following protocols approved by the University of Michigan Institutional Review Board.

Results

Platelets from MPN patients are characterized by surface expression of mutant calreticulin

We examined the localization of CRT proteins on the surface of platelets isolated from blood samples of MPN patients (Supplemental Table 2) or healthy donors that were concurrently processed. The mutant CRT proteins were detected using an antibody (anti-CRT(C_{mut})) directed against 22 amino acids unique to the carboxy domain sequence of MPN-linked mutant CRT proteins [17]. We also used a commercial antibody that binds to the non-mutated amino terminal domain (anti-CRT(N)) of CRT protein present in both the wild-type and mutant CRT proteins. Using flow cytometry, platelets were gated on singlets followed by gating for CD41 (GPIIb) present on the surface of platelets in a heterodimeric complex with CD61 (GPIIIa) [30]. CD62p (P selectin), was used to identify activated platelets [31,32] (**Figure 1A**).

We first examined CD41 and CRT staining patterns in healthy donor platelets by flow cytometry following staining of platelets without fixation/permeabilization (surface) or after fixation and membrane permeabilization (total). Setting detectable protein levels in permeabilized platelets at 100%, a considerable fraction of total CD41 is detected on the surface of platelets (**Figure 1B**). Calreticulin, on the other hand, is predominantly ER-localized, but translocates to cell surface under certain conditions [33]. Our results show low background level staining of CRT with the anti-CRT(N) antibody in non-permeabilized platelets (surface) compared with permeabilized platelets (total), confirming the predominant intracellular localization of wild type CRT in platelets (**Figure 1C**). Compared to healthy donor platelets, we observed significantly higher mean fluorescence intensity (MFI) values of surface staining with both anti-CRT(C_{mut}) (**Figure 1D**) and anti-CRT(N) (**Figure 1E**) antibodies on $CD41^+$ platelets from MPN patients. A similar trend was noted on $CD62p^+$ platelets (activated platelets, **Figures 1F and G**). These results demonstrate that MPN-linked mutant CRT proteins (both Ins5 and Del52) are detectable on the surface of platelets isolated from MPN patients.

Low surface MPL levels in MPN patient platelets

We also measured the levels of MPL protein on platelets isolated from MPN patients expressing mutant CRT proteins and from healthy donors. MPL levels were measured using a commercial anti-MPL antibody (anti-CD110 clone 1.6.1) [34]. We stained unfixed platelets for surface MPL and fixed/permeabilized platelets for total (surface and intracellular) MPL. The respective gating strategies are shown in **Figures 1A** and **2A**. $CD41^+$ platelets isolated from the majority of MPN patients showed lower surface MPL levels than healthy donor platelets, suggesting the specific downmodulation of surface MPL in MPN patient platelets that overrides normal MPL expression variations among individuals (**Figures 2B and 2C**). $CD41^+$ platelets also generally exhibited lower total MPL levels compared to healthy donor platelets processed in parallel (**Figures 2D and 2E**). Platelet lysates from MPN patients compared to healthy donors exhibit a trend

towards lower MPL protein levels, as detected by immunoblotting (**Figure 2F**). Thus, platelets from MPN patients expressing CRT mutants exhibit low surface and total MPL protein levels, which is a potential biomarker for mutant CRT^{+} MPN.

Reduction of total and surface human MPL levels when co-expressed with CRT_{Del52} in Ba/F3 cells

To further investigate whether surface MPL downmodulation is induced by co-expression of MPN-linked CRT mutants, we expressed human MPL protein in the murine pro-B cell line, Ba/F3, together with either wild-type CRT(CRT_{WT}) or Del52 (CRT_{Del52}) or the empty vector control (EV). We observed significant reduction in surface and total MPL protein levels in Ba/F3-MPL CRT_{Del52} cells compared to the CRT_{WT} expressing or EV cells (**Figures 3A-C**).

Two distinct forms of MPL protein are detected (with anti-MPL antibody- 06944 from EMD Millipore) in the lysates upon SDS-PAGE and immunoblotting [35]. Endoglycosidase H (Endo H) cleaves immature N-glycans acquired by glycoproteins in the ER (Endo H-sensitive) but not complex glycans (Endo H-resistant) that have been processed by enzymes within the Golgi complex during glycoprotein trafficking to cell surface. The slower migrating MPL band (just below the 98 kDa marker in **Figures 3D and 3E**) represents the mature MPL protein (M), based on its resistance to Endo H digestion. The faster migrating band (halfway between the 98kDa and 64 kDa markers in **Figures 3D and 3E**) represents the immature MPL (I) band, as Endo H digestion causes its shift to a lower molecular weight (**Figure 3E**). We observe an increase in the fraction of immature MPL in CRT_{Del52}-expressing cells (**Figure 3F**) with a concomitant decrease in the mature protein fraction (**Figure 3G**) when compared to EV or CRT_{WT} expressing cells.

Lysosomal degradation of surface MPL is enhanced in the presence of CRT_{Del52}

We next undertook experiments to better understand the influences of protein degradation upon surface MPL levels in CRT_{Del52} expressing cells as well as the relative prevalence of distinct MPL glycoforms in the presence of CRT_{Del52}. Ba/F3-MPL cells were treated with Bafilomycin A1 (BafA1), an inhibitor of lysosomal acidification, endosomal maturation, and lysosomal degradation [36,37]. BafA1 treatment increased surface MPL levels measured by flow cytometry in the vector control (EV) control cells as well as in CRT_{Del52} expressing Ba/F3-MPL cells (**Figures 4A-B**). However, the rescue of surface MPL upon BafA1 treatment was significantly higher in Ba/F3-MPL cells expressing CRT_{Del52} in comparison to EV cells (**Figure 4C**), indicating increased CRT_{Del52}-mediated MPL degradation. Similar trends were noted when comparing CRT_{Del52} *vs*. CRT_{WT}-overexpressing cells **(Figure S1A)**. Thus, lysosomal degradation of MPL is not specific to CRT_{Del52}-expressing cells, but the presence of CRT_{Del52} appears to enhance MPL degradation via the lysosomal pathway. We further examined a possible additional role of proteasomal degradation in downregulation of surface MPL levels in cells expressing CRT_{Del52}. Ba/F3-MPL cells were treated with proteasomal degradation

inhibitors, MG132 and Bortezomib. Compared to the untreated condition, both EV and CRT_{Del52} expressing cells exhibited a trend towards an increase in the levels of surface MPL, particularly at the lower concentrations of MG132 (0.5 μM to 10 μM) (**Figure 4D**) and upon bortezomib treatment (**Figure 4E**). However, no significant differences were observed in drug-induced changes of surface MPL levels between EV *vs*. CRT_{Del52} cells (**Figures 4D and 4E**). MPL is shown to undergo proteasomal degradation in the presence of TPO [29]. When Ba/F3-MPL EV cells cultured in the absence of IL-3 but in the presence of human TPO were treated with MG132 and Bortezomib, there was a consistent but non-significant increase in cell surface MPL, as observed for Ba/F3-MPL EV cells cultured in the presence of IL-3 but in the absence of TPO (**Figure S1B and S1C**). Overall, it appears that both lysosomal and proteasomal pathways can contribute to MPL degradation, but lysosomal degradation of surface MPL is dominant, particularly in the presence of CRT_{Del52}.

The rescue of surface MPL upon BafA1 treatment was also reflected by an increase in the mature and partially mature MPL fractions in lysates of Ba/F3-MPL CRT_{Del52} as well as in Ba/F3-MPL CRT_{WT} and EV cells, based on immunoblots (**Figure 4F**, lanes 2 compared to 4, 6 compared to 8 and 10 compared to 12 and **Figures 4G and S1D**). On the other hand, 21 μM MG132 treatment induced an increase in mature MPL along with a parallel reduction in the immature MPL levels (band indicated as '**I**' in **Figure 4F**, lanes 2 compared to 3, 6 compared to 7, and 10 compared to 11; **Figures 4G and S1D**) in all the cells. Similar trends are noted in cells treated with 100 nM bortezomib (**Figure S1D**). These effects are observed at the higher concentrations of MG132 or bortezomib (**Figure S1E**) and may correspond to forced MPL exit from the ER and glycan maturation under conditions where ER-associated degradation is blocked via proteasome inhibition.

The immunoblots also show that cells co-expressing CRT_{Del52} and MPL have a lower molecular weight glycoform of mature MPL (**Figure 4F**, lanes 10-13, and **Figure S1D**, lanes 7-12, band labeled M1) compared with EV or CRT_{WT} expressing cells (**Figure 4F**, lanes 2-9, and **Figure S1D**, band labeled M2). This observation is consistent with previous findings that interaction of CRT_{Del52} with MPL prevents the maturation of N117-linked glycan in MPL [16]. Overall, the findings of Figure 4 show that, in cells expressing $CRT_{Del52,}$ BafA1 treatment significantly increases surface (**Figures 4A-C**), partially mature, and total MPL, but not immature MPL (**Figure 4G**). Thus, lysosomal degradation of cell surface and partially mature MPL is likely to underlie the lower cell surface levels of MPL as well as the higher fraction of immature MPL (**Figures 3E-G**) observed in cells expressing $CRT_{Del52.}$ On the other hand, proteasomal inhibition increases the partially mature MPL fraction, but not total MPL (**Figure 4G**), and there is a non-significant increase in surface MPL (**Figures 4D and 4E**).

Inhibiting lysosomal degradation rescues CRT_{Del52} levels

We next assessed pathways relevant to CRT_{Del52} degradation. When Ba/F3-MPL CRT_{Del52} cells were treated with different concentrations of MG132 and bortezomib, we

observed a small non-significant increase in the amounts of CRT_{Del52} in Ba/F3-MPL cells at the low MG132 and bortezomib concentrations. However, CRT_{Del52} levels notably decreased upon treatment with higher concentrations of MG132 (1 μM to 21 μM) (**Figures 5A and 5B**) and bortezomib (50 nM to 1 μM) (**Figures 5C and 5D**) with the levels of CRT_{Del52} being the lowest upon treatment with the highest concentrations of MG132 (21 μM) and bortezomib (1 μM) tested. Thus, higher concentrations of proteasomal inhibitors promote CRT_{Del52} degradation in Ba/F3-MPL cells.

We further examined changes to cell surface CRT_{Del52} levels in Ba/F3 treated with 21 μM MG132 or 100 nM BafA1 or both. Under all conditions, flow cytometric analyses using the anti-CRT(C_{mut}) antibody [17] indicated low to undetectable surface expression of CRT_{Del52} in the absence of MPL (**Figure 5E**). On the other hand, cell surface CRT_{Del52} is better detectable in cells expressing MPL but neither MG132 nor BafA1 significantly affected surface CRT_{Del52} expression (**Figures 5E and 5F**). Since MPL and CRT_{Del52} are known to interact at the cell surface [5], it is somewhat surprising that the BafA1 treatment rescues surface MPL (**Figures 4B and 4C**) but does not affect surface CRT_{Del52} (**Figure 5F**). It is possible that while the partially mature form of MPL and CRT_{Del52} are internalized from the cell surface as a complex, the proteins are not necessarily recycled to plasma membrane as a complex. Whereas MPL recycling rescues surface MPL levels, CRT_{Del52} is mostly secreted as indicated by our findings below. Notably however, as observed for MPL (**Figure 4**), BafA1 treatment increased cellular (lysate) CRT_{Del52} levels in Ba/F3-MPL cells when compared to untreated cells (CRT_{Del52} blot in **Figure 5G**, lanes 9 *vs.* 11). BafA1-mediated increase in CRT_{Del52} levels was also observed in the Ba/F3 cells in the absence of MPL co-expression; however, the rescue of cellular CRT_{Del52} levels is only significant in the cells co-expressing MPL (**Figure 5H**). On the other hand, treatment with MG132 (21 μM) promoted CRT_{Del52} degradation independently of MPL co-expression (CRT_{Del52} blot in **Figure 5G,** lanes 5 *vs.* 6 and lanes 9 *vs.*10 and **Figure 5H**).

Paired comparisons of the CRT_{Del52} band intensities in the presence of MG132 alone with the MG132+BafA1 condition showed increased recovery of CRT_{Del52} in the MG132+BafA1 condition, which is statistically significant in BaF3-CRT_{Del52} cells co-expressing MPL but shows similar trends in the absence of MPL (**Figure 5I**). Similar trends are also noted in a representative experiment comparing 100 nM bortezomib alone with the combination of 100 nM each of bortezomib and BafA1 (**Figure S1D**). Thus, high concentrations of proteasome inhibitors may increase lysosomal degradation of cellular CRT_{Del52}. There is precedence for such effects of proteasome inhibitors in the literature [38].

To compare the effects of the degradation inhibitors upon CRT_{Del52} secretion, we immunoprecipitated CRT_{Del52} using the anti-CRT(C_{mut}) antibody [17] from the culture supernatant of Ba/F3 cells following treatments with MG132 and/or BafA1. As shown by the representative blots, the absence of bands following IP from EV or CRT_{WT} expressing control cells (**Figure 5J**, lanes 1 and 2) demonstrated the specificity of IP of

CRT_{Del52} from Ba/F3 cells expressing CRT_{Del52}. BafA1 treatment resulted in a trend towards rescue of secreted CRT_{Del52} in culture supernatant of Ba/F3 cells irrespective of MPL co-expression (**Figure 5J**, lanes 5 and 9, and **Figure 5K**). MG132 treatment resulted in loss of secreted CRT_{Del52} in the absence of MPL (**Figures 5J and 5K**). The combination of BafA1 treatment with MG132 showed non-significant changes to secreted CRT_{Del52} in the culture supernatants of Ba/F3 cells (with or without MPL co-expression) when compared to untreated cells (**Figure 5K**) and to the cells treated with MG132 alone (**Figure 5L**).

CRT_{Del52} exhibits increased lysosomal localization compared with CRT_{WT} and increases the fraction of MPL in lysosomes

We used a microscopy-based approach to probe lysosomal localization of CRT_{Del52} in BafA1-treated cells. HEK293T cells were transfected to overexpress human MPL together with either CRT_{WT} or CRT_{Del52} and processed for confocal microscopy. Anti-CRT(C_{mut}) was used to stain CRT_{Del52} whereas the CRT_{WT} protein was stained with anti-CRT(N). Mutant CRT is previously shown to colocalize with markers of Golgi apparatus [5] while CRT_{WT} colocalizes with ER markers [3,5]. In addition to the perinuclear Golgi-like localization described earlier [5], we observed a vesicular or punctate pattern of CRT_{Del52} localization in HEK cells (**Figure 6A**)**,** which has also been reported earlier [9]. This was observed under both the untreated and BafA1-treated conditions. CRT_{WT}, on the other hand, exhibited a more homogenous ER-like subcellular localization with fewer puncta, if any (**Figure 6A**). MPL also showed a vesicular/punctate localization besides the Golgi-like perinuclear and membrane localization, under both untreated and BafA1-treated conditions (**Figure 6A**). Lysosomes were stained with lysosomal-associated membrane protein 1 (LAMP1). Object-based quantification was undertaken using CellProfiler on the BafA1-treated cells (**Figures 6B-6F**). A significantly higher number of puncta were observed for CRT_{Del52} compared to CRT_{WT} (**Figure 6B**). CRT_{Del52} expressing cells also showed a significantly higher number of MPL puncta (**Figure 6C**) and a significantly higher colocalization of MPL and CRT_{Del52} puncta (**Figure 6D**). CRT_{Del52} and MPL puncta displayed colocalization within or in close proximity to the LAMP1 structures (**Figure 6A,** arrowheads in zoomed inset). Compared to CRT_{WT}, a significantly higher fraction of CRT_{Del52} puncta colocalized with LAMP1-positive lysosomal structures (**Figure 6E**). In agreement with this, a significantly higher fraction of lysosomes (LAMP1 structures) displayed colocalization with CRT_{Del52} and MPL puncta (**Figure 6F**) compared with CRT_{WT}. The increased lysosomal localization of CRT_{Del52} supports our finding that the lysosomal pathway is relevant to the regulation of cellular CRT_{Del52} levels (**Figure 5**). Furthermore, enhanced lysosomal localization of MPL in CRT_{Del52} expressing cells supports our finding of CRT_{Del52}-mediated increase in lysosomal degradation of surface MPL (**Figures 4C,4F and 4G**).

mTOR inhibition reduces cytokine-independent proliferation mediated by CRT_{Del52}

Figures 4 and 5 show that CRT_{Del52} and MPL are degraded via the lysosomal pathway more significantly in the presence of one another, and inhibition of lysosomal

degradation rescues both proteins. Based on these results, we examined whether direct activation of lysosomal degradation using FDA-approved clinical drugs could promote CRT_{Del52} and MPL degradation and interfere with the cell proliferative effects of CRT_{Del52}. For this, we used rapamycin and everolimus, both of which are the inhibitors of mammalian target of rapamycin (mTOR), a protein kinase that inhibits autophagy and promotes cell growth and anabolism in response to several growth factors, nutrients, and other factors [39]. We expected that one effect of these drugs would be the induction of lysosomal degradation. Ba/F3-MPL EV cells cultured in the presence of IL-3 generally show normal growth patterns upon treatment with either 50 nM or 100 nM rapamycin (**Figures 7A and 7B**) or 100 nM everolimus (**Figures 7C and 7D**). A low inhibition of proliferation of Ba/F3-MPL EV cells was measured at early time points upon treatment with rapamycin or everolimus (**Figures 7B and 7D**) which could result from the inhibition of IL-3-dependent signaling pathway by mTOR inhibitors [40]. However, the EV cells recover from the effects of mTOR inhibitors at later time points (**Figures 7B and 7D**). In contrast, Ba/F3-MPL CRT_{Del52} cells show significantly reduced cytokine-independent proliferation upon treatment with rapamycin (**Figures 7E and 7F**) and everolimus (**Figures 7G and 7H**). A significant reduction of cytokine-independent proliferation was observed after treatment of Ba/F3-MPL CRT_{Del52} cells with rapamycin starting at Day 2 (**Figure 7F**) as well as with 100 nM everolimus starting at Day 1 (**Figure 7H**). In contrast, mTOR inhibitors have smaller and largely non-significant effects on proliferation of Ba/F3-MPL EV cells cultured in the presence of TPO (**Figures 7I** and **7J**). Everolimus-mediated inhibition of Ba/F3-MPL CRT_{Del52} cell proliferation was accompanied by an increase in the fraction of cells in the early apoptotic stage and a concomitant decrease in the fraction of cells in the S phase of cell cycle (**Figures S2A-E**).

To examine whether reduced proliferation of Ba/F3-MPL cells treated with rapamycin and everolimus is mediated by enhanced degradation of MPL and/or CRT_{Del52}, we measured cellular CRT_{Del52} and MPL levels in the lysates of untreated or treated cells at different time points. Immunoblots confirmed that at least at earlier time points (lanes highlighted by boxes), both CRT_{Del52} and MPL levels are lower in cells treated with rapamycin (**Figure 7K**), lanes 3 to 6 and lanes 7 to 10 corresponding to lysates from days 1 and 2, respectively, after the start of drug treatments) and everolimus (**Figure 7L**, lanes 7 to 10 and lanes 14 to 17 corresponding to lysates from days 2 and 3, respectively, after the start of drug treatments) compared to untreated cells. Everolimus-mediated reduction in CRT_{Del52} levels was also observed for secreted CRT_{Del52} in the media, based on immunoprecipitation analyses (**Figure 7M**). Thus, reduction in cellular CRT_{Del52} and MPL levels triggered by treatment with mTOR-inhibiting (lysosomal degradation-activating) drugs could in part explain the observed reduction in cytokine-independent proliferation of Ba/F3-MPL CRT_{Del52} cells in the presence of rapamycin and everolimus.

Primary $CD34^+$ cells from MPN patients demonstrate lower colony-forming capacity and reduced differentiation following treatment with everolimus

To check the susceptibility of primary $CD34^+$ cells from CRT-mutated MPN patients to mTOR inhibition, colony forming unit (CFU) assays were performed with $CD34^+$ cells isolated from bone marrow samples of MPN patients (Supplemental Table 3) or from healthy donor leukopaks. In the first set of experiments, the $CD34^+$ cells were either left untreated or pre-treated with everolimus for 24 hours before plating (**Figure 7N,** pre-treatment). In subsequent experiments, everolimus was incorporated within the plating media (**Figure 7O,** continuous treatment). Compared to colony counts under untreated conditions, MPN patient $CD34^+$ cells exhibited a decrease in the number of CFUs following pre-treatment with 50 nM everolimus, but the reduction was non-significant (**Figure 7N**, n=6). Under more stringent conditions involving continuous exposure to 50 nM everolimus (**Figure 7O,** n=6), a significant decrease in the number of CFUs derived from MPN patient $CD34^+$ cells was observed when compared to untreated cells. There was significant heterogeneity in the measured response which included a heterogenous group of available patient samples in different disease states (Supplemental Table 3). However, healthy donor $CD34^+$ cells exhibited no to little effects of pre-treatment (n=4) or continuous treatment (n=3) with 50 nM everolimus when compared to untreated healthy $CD34^+$ cells (**Figures 7N and 7O**). Furthermore, when differentiated into megakaryocytes, $CD34^+$ cells from MPN patients showed reduced fractions of differentiated $CD41^+CD42a^+$ cells in the presence of everolimus, but this was not observed with healthy donor $CD34^+$ cells (**Figure 7Q**). Thus, despite expected variabilities in primary human samples, the results from figure 7 clearly indicate that mutant CRT expressing BaF3-MPL cells and primary $CD34^+$ cells from MPN patients are more susceptible to mTOR inhibition compared to healthy donor $CD34^+$ cells. The parallel loss in CRT_{Del52} and MPL is consistent with the model that mTOR-mediated activation of the autophagy/lysosomal pathway is detrimental for CRT_{Del52}-mediated cell proliferation.

Discussion

Our results indicate a significant increase in localization of CRT mutants on the surface of both the resting ($CD41^+$) and activated platelets ($CD62p^+$) isolated from MPN patients when compared to healthy donor platelets (**Figures 1D-G**), consistent with previous findings in other cells [8-10,16]. While early studies have reported downregulation of surface MPL on platelets in ET, PV, and MF patients [41,42], whether patients with CRT mutations also have low MPL levels is unknown. Our findings indicate that platelets from most of the MPN patients with CRT mutations exhibit low MPL/TPOR levels when compared to healthy donor platelets (**Figure 2**). These findings prompted studies of the role of proteasomal and lysosomal degradation pathways in regulating the dynamics of MPL and mutant CRT proteins in MPNs. The low surface and mature MPL levels measured in Ba/F3 cells expressing both MPL and CRT_{Del52} confirmed that the observed MPL downmodulation is more acute in the cells expressing mutant CRT proteins (**Figure 3**).

Mature MPL is suggested to be targeted for degradation by both the lysosomal and proteasomal degradation pathways in response to TPO [28,29]. On the other hand, MPL downmodulation in Ba/F3-MPL cells expressing the JAK2V617F mutant was attributed to increased ubiquitination and degradation of the receptor by the proteasomal degradation pathway [43]. By analogy to these prior findings, we suggest a model wherein low MPL levels on the cell surface in mutant CRT-expressing cells result from MPL signaling activated by mutant CRT proteins followed by internalization and lysosomal degradation of MPL-mutant CRT complexes. Notably, lysosomal degradation rather than proteasomal degradation of these complexes is prominently induced in the context of the CRT mutants**.** In support of this model (see **visual abstract**), we find that inhibition of lysosomal acidification markedly increases cellular CRT_{Del52} levels, particularly in the presence of MPL (**Figures 5G and 5H**). Additionally, lysosomal degradation of cell-surface MPL becomes more prominent (**Figure 4C**) and an increased lysosomal localization of MPL is observed when CRT_{Del52} is co-expressed (**Figure 6**). Additionally, synergistic increase of both MPL and CRT_{Del52} levels is observed upon inhibition of lysosomal degradation (**Figures 4 and 5**).

In contrast to the measured accumulation of cellular CRT_{Del52} and cell-surface MPL following treatment with the inhibitor of lysosomal degradation, BafA1, drug-mediated inhibition of proteasomal degradation reduces cellular CRT_{Del52} levels while not increasing secreted mutant calreticulin levels (**Figures 5A-D, 5G-K and S1D**). This observation suggests that proteasomal inhibitors enhance degradation of CRT_{Del52}. These findings are consistent with the observed decrease in mutant CRT protein levels following inhibition of proteasomal degradation reported in an earlier study [7]. Reduced CRT_{Del52} levels following inhibition of proteasomal degradation are likely caused by enhanced CRT_{Del52} degradation via activation of autophagy/lysosomal pathway [38] (**Figure 5I**). Recent studies have shown that the proteasomal pathway is upregulated in mutant CRT-expressing cells from MPN patients [44]. Treatment with the proteasomal inhibitor, bortezomib, inhibits the proliferation of mutant CRT-expressing HSCs and megakaryocytes [44,45], which is attributed to the combined targeting of the proteasome and an ER stress response prevalent in cells expressing CRT_{Del52}. While these studies did not show the effect of proteasomal inhibitors on the expression levels of CRT mutants, it is likely that the proliferation-suppressive effects of the proteasomal inhibitors are, at least in part, driven by their ability to induce CRT_{Del52} degradation.

In contrast to MPL protein levels, expression of MPN-linked mutant CRT proteins has been associated with increased MPL transcription [7,46]. In one of these studies, enhanced MPL transcription has been attributed to enhanced binding of ERp57 and transcription factor Fli1 on MPL promoter in CRT_{Del52} expressing cells [46]. While MPL protein levels were not measured in those studies, the data in **Figure 2** of this study indicate a dominant loss of MPL expression in platelets despite any gain in mRNA expression, further supporting the model that protein degradation contributes to the low measured MPL protein levels. Downregulation of MPL protein levels despite increased

MPL mRNA expression was also observed in Ba/F3-MPL cells expressing the JAK2V617F mutant [43].

mTOR activity plays a crucial role in regulating lysosomal function by regulating lysosomal biogenesis, lysosomal positioning, and activity of lysosomal proteins [47]. mTOR inhibition has been correlated to enhanced lysosomal degradation via different mechanisms including enhanced lysosomal biogenesis [48] or enhanced lysosomal acidification through assembly of active V-ATPase at lysosomal membranes [49]. mTOR inhibitors, rapamycin and everolimus, inhibit proliferation and survival of cancer cells [50,51]. We further show here that treatments with these drugs, suppress cytokine-independent proliferation of CRT_{Del52} expressing Ba/F3-MPL cells (**Figures 7A-J**). The drugs also induce a decrease in the levels of cellular CRT_{Del52} and MPL and secreted $CRT_{Del52,}$ which is readily detectable at early time points after drug treatment (**Figures 7K-7M**). We also observe a decrease in the number of CFUs recovered from $CD34^+$ cells isolated from MPN patients following treatment with everolimus and a reduction in $CD34^+$ cell differentiation to megakaryocytes (**Figures 7N-7Q**). In contrast, everolimus treatment had no measured impact on colony growth or differentiation of $CD34^+$ cells from healthy donors (**Figures 7N-7Q**).

Overall, our findings demonstrate the importance of cellular degradation pathways in regulation of MPL and mutant CRT protein levels, which are the two major factors controlling oncogenesis in mutant CRT-linked MPNs. Everolimus (or RAD001) has been approved as an anti-cancer drug for treatment of breast cancer, renal cell carcinoma, and certain types of pancreatic and lung cancers, etc. (www.cancer.gov/about-cancer/treatment/drugs/everolimus). Some studies have indicated mTOR pathway inhibitors as potential drugs for treatment of MPNs [52,53]. The combination of an mTOR inhibitor, BEZ235 and JAK2 inhibitor, Ruxolitinib, showed synergistic effects in the treatment of JAK2V617F mice models of MPNs [54]. Our studies suggest that mTOR inhibitors are promising targets for treatment of MPN patients expressing CRT mutants and highlight their therapeutic potential.

Acknowledgments

We are grateful to all the donors and patients who volunteered to donate blood and/or bone marrow samples for this work. We thank Amanda Prieur from the University of Michigan Platelet Physiology and Pharmacology Core for collecting healthy donor blood samples. We thank Polk Avery from Talpaz lab for coordinating and collecting MPN patient blood and bone marrow samples. This work was funded by National Institute of Health grants (R01 AI123957) to MR and the University of Michigan Fast Forward Protein Folding Diseases Initiative.

Author Contributions

AK and AV designed and performed experiments, analyzed data, wrote the original draft and edited the manuscript. MK collected patient blood and bone marrow samples, purified platelets and edited the manuscript. MT is the director of MPN repository at the University of Michigan. MR designed and supervised the study, obtained funding, analyzed data, and wrote, and edited the manuscript.

Conflicts of Interest

Dr. Moshe Talpaz serves as advisory board member for Sierra Oncology, Bristol Myers Squibb, Sumitomo, and GlaxoSmithKline/Pfizer and has received research support from Bristol Myers Squibb, Novartis, Sumitomo and Morphosys.

References

1. Campbell PJ, Green AR. The Myeloproliferative Disorders. *N Engl J Med*. 2006;355(23):2452-2466. doi:10.1056/NEJMra063728

2. Spivak JL. Myeloproliferative Neoplasms. *N Engl J Med*. 2017;376(22):2168-2181. doi:10.1056/NEJMra1406186

3. Klampfl T, Gisslinger H, Harutyunyan AS, et al. Somatic Mutations of Calreticulin in Myeloproliferative Neoplasms. *N Engl J Med*. 2013;369(25):2379-90. doi:10.1056/NEJMoa1311347

4. Nangalia J, Massie CE, Baxter EJ, et al. Somatic CALR mutations in myeloproliferative neoplasms with nonmutated JAK2. *N Engl J Med*. 2013;369(25):2391-2405. doi:10.1056/NEJMoa1312542

5. Masubuchi N, Araki M, Yang Y, et al. Mutant calreticulin interacts with MPL in the secretion pathway for activation on the cell surface. *Leukemia*. 2020;34(2):499-509. doi:10.1038/s41375-019-0564-z

6. Arshad N, Cresswell P. Tumor-associated calreticulin variants functionally compromise the peptide loading complex and impair its recruitment of MHC-I. *J Biol Chem*. 2018;293(25):9555-9569. doi:10.1074/jbc.RA118.002836

7. Han L, Schubert C, Köhler J, et al. Calreticulin-mutant proteins induce megakaryocytic signaling to transform hematopoietic cells and undergo accelerated degradation and Golgi-mediated secretion. *J Hematol Oncol*. 2016;9(1):1-14. doi:10.1186/s13045-016-0275-0

8. Liu P, Zhao L, Loos F, et al. Immunosuppression by Mutated Calreticulin Released from Malignant Cells. *Mol Cell*. 2020;77(4):748-760.e9. doi:10.1016/j.molcel.2019.11.004

9. Pecquet C, Papadopoulos N, Balligand T, et al. Secreted Mutant Calreticulins As Rogue Cytokines in Myeloproliferative Neoplasms. *Blood*. 2023;141(8):917-929. doi:10.1182/blood.2022016846

10. Araki M, Yang Y, Masubuchi N, et al. Activation of the thrombopoietin receptor by mutant calreticulin in CALR-mutant myeloproliferative neoplasms. *Blood*. 2016;127(10):1307-1316. doi:10.1182/blood-2015-09-671172

11. Chachoua I, Pecquet C, El-Khoury M, et al. Thrombopoietin receptor activation by myeloproliferative neoplasm associated calreticulin mutants. *Blood*. 2016;127(10):1325-1335. doi:10.1182/blood-2015-11-681932

12. Elf S, Abdelfattah NS, Chen E, et al. Mutant Calreticulin Requires Both Its Mutant C-terminus and the Thrombopoietin Receptor for Oncogenic Transformation. *Cancer Discov*. 2016;6(4):368-381. doi:10.1158/2159-8290.CD-15-1434

13. Marty C, Pecquet C, Nivarthi H, et al. Calreticulin mutants in mice induce an MPL-dependent thrombocytosis with frequent progression to myelofibrosis. *Blood*. 2016;127(10):1317-1324. doi:10.1182/blood-2015-11-679571

14. Elf S, Abdelfattah NS, Baral AJ, et al. Defining the requirements for the pathogenic interaction between mutant calreticulin and MPL in MPN. *Blood*. 2018;131(7):782-786. doi:10.1182/blood-2017-08-800896

15. Papadopoulos N, Nedelec A, Derenne A, et al. Oncogenic CALR mutant C-terminus mediates dual binding to the thrombopoietin receptor triggering complex dimerization and activation. *Nat Commun*. Apr 5 2023;14(1):1881. doi:10.1038/s41467-023-37277-3

16. Pecquet C, Chachoua I, Roy A, et al. Calreticulin mutants as oncogenic rogue chaperones for TpoR and traffic-defective pathogenic TpoR mutants. *Blood*. 2019;133(25):2669-2681. doi:10.1182/blood-2018-09-874578

17. Venkatesan A, Geng J, Kandarpa M, et al. Mechanism of mutant calreticulin-mediated activation of the thrombopoietin receptor in cancers. *J Cell Biol*. 2021;220(7):e202009179-e202009179. doi:10.1083/jcb.202009179

18. Desikan H, Kaur A, Pogozheva ID, Raghavan M. Effects of calreticulin mutations on cell transformation and immunity. *J Cell Mol Med*. Apr 2023;27(8):1032-1044. doi:10.1111/jcmm.17713

19. Debili N, Wendling F, Cosman D, et al. The Mpl Receptor Is Expressed in the Megakaryocytic Lineage From Late Progenitors to Platelets. *Blood*. 1995;85(2):391-401. doi:10.1182/blood.V85.2.391.391

20. Qian H, Buza-Vidas N, Hyland CD, et al. Critical Role of Thrombopoietin in Maintaining Adult Quiescent Hematopoietic Stem Cells. *Cell Stem Cell*. 2007;1(6):671-684. doi:10.1016/j.stem.2007.10.008

21. Wendling F, Maraskovsky E, Debili N, et al. c-Mpl ligand is a humoral regulator of megakaryocytopoiesis. *Nature*. 1994;369(6481):571-574. doi:10.1038/369571a0

22. Balligand T, Achouri Y, Pecquet C, et al. Knock-in of murine Calr del52 induces essential thrombocythemia with slow-rising dominance in mice and reveals key role of Calr exon 9 in cardiac development. *Leukemia*. 2020;34(2):510-521. doi:10.1038/s41375-019-0538-1

23. Shide K, Kameda T, Yamaji T, et al. Calreticulin mutant mice develop essential thrombocythemia that is ameliorated by the JAK inhibitor ruxolitinib. *Leukemia*. 2017;31(5):1136-1144. doi:10.1038/leu.2016.308

24. Benlabiod C, Cacemiro MDC, Nedelec A, et al. Calreticulin del52 and ins5 knock-in mice recapitulate different myeloproliferative phenotypes observed in patients with MPN. *Nat Commun*. Sep 28 2020;11(1):4886. doi:10.1038/s41467-020-18691-3

25. Varghese LN, Defour J-P, Pecquet C, Constantinescu SN. The thrombopoietin receptor: structural basis of traffic and activation by ligand, mutations, agonists, and mutated calreticulin. *Front Endocrinol*. 2017;8:59. doi:10.3389/fendo.2017.00059

26. Dahlen DD, Broudy VC, Drachman JG. Internalization of the thrombopoietin receptor is regulated by 2 cytoplasmic motifs. *Blood*. 2003;102(1):102-108. doi:10.1182/blood-2002-11-3468

27. Fielder PJ, Gurney AL, Stefanich E, et al. Regulation of Thrombopoietin Levels by c-mpl–Mediated Binding to Platelets. *Blood*. 1996;87(6):2154-2161. doi:10.1182/blood.V87.6.2154.bloodjournal8762154

28. Hitchcock IS, Chen MM, King JR, Kaushansky K. YRRL motifs in the cytoplasmic domain of the thrombopoietin receptor regulate receptor internalization and degradation. *Blood*. 2008;112(6):2222-2231. doi:10.1182/blood-2008-01-134049

29. Saur SJ, Sangkhae V, Geddis AE, Kaushansky K, Hitchcock IS. Ubiquitination and degradation of the thrombopoietin receptor c-Mpl. *Blood*. 2010;115(6):1254-1263. doi:10.1182/blood-2009-06-227033

30. Phillips DR, Charo IF, Parise LV, Fitzgerald LA. The Platelet Membrane Glycoprotein IIb-IIIa Complex. *Blood*. 1988;71(4):831-843. doi:10.1182/blood.V71.4.831.831

31. Leytin V, Mody M, Semple JW, Garvey B, Freedman J. Flow cytometric parameters for characterizing platelet activation by measuring P-selectin (CD62) expression: theoretical consideration and evaluation in thrombin-treated platelet populations. *Biochem Biophys Res Commun*. Mar 5 2000;269(1):85-90. doi:10.1006/bbrc.2000.2255

32. McEver RP. GMP-140: a receptor for neutrophils and monocytes on activated platelets and endothelium. *J Cell Biochem*. 1991;45(2):156-161. doi:10.1002/jcb.240450206

33. Raghavan M, Wijeyesakere SJ, Peters LR, Del Cid N. Calreticulin in the immune system: ins and outs. *Trends Immunol*. 2013;34(1):13-21. doi:10.1016/j.it.2012.08.002

34. Abbott C, Huang G, Ellison AR, et al. Mouse Monoclonal Antibodies Against Human c-Mpl and Characterization for Flow Cytometry Applications. *Hybridoma*. 2010;29(2):103-113. doi:10.1089/hyb.2009.0095

35. Royer Y, Staerk J, Costuleanu M, Courtoy PJ, Constantinescu SN. Janus Kinases Affect Thrombopoietin Receptor Cell Surface Localization and Stability*. *J Biol Chem*. 2005;280(29):27251-27261. doi:10.1074/jbc.M501376200

36. Wang R, Wang J, Hassan A, Lee C-H, Xie X-S, Li X. Molecular basis of V-ATPase inhibition by bafilomycin A1. *Nat Commun*. 2021;12(1):1782. doi:10.1038/s41467-021-22111-5

37. Yamamoto A, Tagawa Y, Yoshimori T, Moriyama Y, Masaki R, Tashiro Y. Bafilomycin A1 prevents maturation of autophagic vacuoles by inhibiting fusion between autophagosomes and lysosomes in rat hepatoma cell line, H-4-II-E cells. *Cell Struct Funct*. 1998;23(1):33-42. doi:10.1247/csf.23.33

38. Li C, Wang X, Li X, et al. Proteasome Inhibition Activates Autophagy-Lysosome Pathway Associated With TFEB Dephosphorylation and Nuclear Translocation. *Front Cell Dev Biol*. 2019;7:170. doi:10.3389/fcell.2019.00170

39. Kim YC, Guan K-L. mTOR: a pharmacologic target for autophagy regulation. *JCI*. 2015;125(1):25-32. doi:10.1172/JCI73939

40. Cruz R, Hedden L, Boyer D, Kharas MG, Fruman DA, Lee-Fruman KK. S6 kinase 2 potentiates interleukin-3-driven cell proliferation. *J Leukoc Biol*. 2005;78(6):1378-1385. doi:10.1189/jlb.0405225

41. Horikawa Y, Matsumura I, Hashimoto K, et al. Markedly reduced expression of platelet c-mpl receptor in essential thrombocythemia. *Blood*. Nov 15 1997;90(10):4031-8.

42. Moliterno AR, Hankins WD, Spivak JL. Impaired expression of the thrombopoietin receptor by platelets from patients with polycythemia vera. *N Engl J Med*. Feb 26 1998;338(9):572-80. doi:10.1056/NEJM199802263380903

43. Pecquet C, Diaconu CC, Staerk J, et al. Thrombopoietin receptor down-modulation by JAK2 V617F: restoration of receptor levels by inhibitors of pathologic JAK2 signaling and of proteasomes. *Blood*. May 17 2012;119(20):4625-35. doi:10.1182/blood-2011-08-372524

44. Jutzi JS, Marneth AE, Jimenez-Santos MJ, et al. CALR-mutated cells are vulnerable to combined inhibition of the proteasome and the endoplasmic reticulum stress response. *Leukemia*. Feb 2023;37(2):359-369. doi:10.1038/s41375-022-01781-0

45. Foßelteder J, Pabst G, Sconocchia T, et al. Human gene-engineered calreticulin mutant stem cells recapitulate MPN hallmarks and identify targetable vulnerabilities. *Leukemia*. Apr 2023;37(4):843-853. doi:10.1038/s41375-023-01848-6

46. Pronier E, Cifani P, Merlinsky TR, et al. Targeting the CALR interactome in myeloproliferative neoplasms. *JCI Insight*. Nov 15 2018;3(22):e122703. doi:10.1172/jci.insight.122703

47. Puertollano R. mTOR and lysosome regulation. *F1000Prime Rep*. 2014;6:52. doi:10.12703/P6-52

48. Settembre C, Zoncu R, Medina DL, et al. A lysosome-to-nucleus signalling mechanism senses and regulates the lysosome via mTOR and TFEB. *EMBO J*. Mar 7 2012;31(5):1095-108. doi:10.1038/emboj.2012.32

49. Ratto E, Chowdhury SR, Siefert NS, et al. Direct control of lysosomal catabolic activity by mTORC1 through regulation of V-ATPase assembly. *Nat Commun*. Aug 17 2022;13(1):4848. doi:10.1038/s41467-022-32515-6

50. Guertin DA, Sabatini DM. An expanding role for mTOR in cancer. *Trends Mol Med*. Aug 2005;11(8):353-61. doi:10.1016/j.molmed.2005.06.007

51. Sabatini DM. mTOR and cancer: insights into a complex relationship. *Nat Rev Cancer*. Sep 2006;6(9):729-34. doi:10.1038/nrc1974

52. Guglielmelli P, Barosi G, Rambaldi A, et al. Safety and efficacy of everolimus, a mTOR inhibitor, as single agent in a phase 1/2 study in patients with myelofibrosis. *Blood*. Aug 25 2011;118(8):2069-76. doi:10.1182/blood-2011-01-330563

53. Vannucchi AM, Harrison CN. Emerging treatments for classical myeloproliferative neoplasms. *Blood*. Feb 9 2017;129(6):693-703. doi:10.1182/blood-2016-10-695965

54. Bartalucci N, Tozzi L, Bogani C, et al. Co-targeting the PI3K/mTOR and JAK2 signalling pathways produces synergistic activity against myeloproliferative neoplasms. *J Cell Mol Med*. Nov 2013;17(11):1385-96. doi:10.1111/jcmm.12162

Figure Legends

Figure 1: Platelets from MPN patients are characterized by cell surface expression of mutant calreticulin. Platelets were isolated from blood samples of mutant CRT-expressing MPN patients and healthy controls. **(A)** Gating strategy used for the analysis of unfixed $CD41^+$ and $CD62p^+$ platelets by flow cytometry. **(B-C)** Bar graphs indicate flow cytometry-based detection of staining for CD41 **(B)** and CRT (detected using an N-domain-specific antibody, anti-CRT(N)) **(C)** on healthy donor platelets either without fixation (surface) or after fixation and permeabilization (total) (n=7). Relative mean fluorescence intensity (MFI) values after surface and total staining are plotted, assuming MFI values for total CD41 (B) or total CRT (C) as 100%. Paired t-tests were used for determining the statistical significance. **(D-G)** Flow cytometry-based detection of surface CRT on unfixed $CD41^+$ **(D&E)** and unfixed $CD62p^+$ **(F&G)** platelets. Representative histograms and bar graphs show MFI of surface CRT detected on platelets by either mutant CRT-specific antibody (anti-CRT (C_{mut})) or anti-CRT (N) antibody. MPN patient and healthy donor (HC) platelet samples that were processed simultaneously were analyzed as pairs for these measurements. Data are separately analyzed for Del52 (n=13 for $CD41^+$ platelets and n=9 for $CD62p^+$ platelets) and Ins5 (n=8 for $CD41^+$ platelets and n=8 for $CD62p^+$ platelets) patient samples. The error bars show the standard error of the mean (SEM). Statistical significance indicated by p-values was determined using GraphPad Prism and paired t-test analyses. The heterogeneity of CD41 expression in the representative panel shown in A most likely relates to the limiting use of antibody, as similar results were obtained based on $CD41^{hi}$-gating *vs.* gating on all single cells.

Figure 2: Downmodulation of MPL in MPN patient platelets. (A) Gating strategy used for the analysis of fixed and permeabilized platelets by flow cytometry. **(B and D)** Representative histograms show surface (B) or total (D) MPL staining with anti-MPL antibody on MPN patient (MPN) platelets (red histograms) or same-day healthy control (HC) platelets (blue histograms) in unfixed (B) or fixed and permeabilized (D) platelets. **(C and E)** The MFI values of surface (C; n=12 for Del52 and n=7 for Ins5 samples) and total (E; n=19 for Del52 and n=7 for Ins5 samples) MPL staining on platelets. Each dot in **(C)** and **(E)** represents the MFI value for an individual MPN or HC platelet sample, while the lines connect pairs of HC and MPN patient samples that were processed in parallel. Statistical significance indicated by p-values were determined using GraphPad Prism and paired t-test analyses. **(F)** Representative blots showing MPL and mutant CRT protein levels in the lysates of healthy control or MPN patient platelets subjected to SDS-PAGE under reducing conditions followed by immunoblotting. Anti-MPL and anti-CRT(C_{mut}) antibodies were used for detection of MPL and mutant CRT proteins, respectively. GAPDH blot shows relative loading of lysates. The heterogeneity of CD41 expression in the representative panel shown in A most likely relates to the limiting use of antibody, as similar results were obtained based on $CD41^{hi}$-gating *vs.* gating on all single cells.

Figure 3: Reduction of total and surface human MPL levels when co-expressed with CRT_{Del52} in Ba/F3 cells. IL-3-dependent murine Ba/F3 cells were transduced for co-expression of human MPL and either WT human CRT (CRT_{WT}) or mutant human CRT (CRT_{Del52}) protein. Ba/F3 cells expressing only human MPL protein (Empty Vector, EV) were included as controls. **(A)** Representative histograms show surface and total MPL staining detected by flow cytometry in Ba/F3-MPL cells expressing either MPL alone or MPL along with CRT_{WT} or CRT_{Del52} as indicated. **(B)** Bar graphs show quantifications of MFI values of surface MPL **(B)** and total MPL **(C)** measured by flow cytometry in CRT_{WT} or CRT_{Del52} expressing cells normalized to the MFI values of EV cells within the same experiments. The data points represent measurements taken in 38 (B) and 25 (C) independent experiments using cells from ~8 different retroviral infections. P-values show statistical significance determined by paired t-test analyses using GraphPad Prism. **(D and E)** Representative immunoblots (D, n=14 and E, n=3) showing the levels of total MPL protein in Ba/F3 cells co-expressing either CRT_{Del52} or CRT_{WT} compared to empty vector (EV) control cells (D) and without or with Endo H digestion (E). GAPDH is shown for loading controls. Top and bottom bands in the MPL blots represent the mature (M) and immature (I) forms of MPL proteins, respectively. **(F and G)** Bar graphs show fraction of immature (F) and mature (G) human MPL protein in EV, CRT_{WT} and CRT_{Del52}-expressing cells, quantified from intensities of the mature and immature MPL

bands from the immunoblots using image J software normalized to the intensities of GAPDH bands. Paired t-tests were used in GraphPad Prism to determine statistical significance, indicated by p-values.

Figure 4: Inhibition of lysosomal acidification rescues cell surface levels of MPL protein more significantly in the presence of CRT_{Del52}. (A-C) Murine Ba/F3-MPL control (EV) cells or those expressing CRT_{Del52} were treated with 100 nM Bafilomycin A1 (BafA1) for 4h in media with IL-3. Untreated cells are included for comparison. Surface MPL levels were detected by flow cytometry. (A) Representative histograms of surface MPL levels with and without BafA1 treatment in both the cell lines. (B) Averaged MFI for surface MPL levels after BafA1 treatment, plotted as a ratio to the levels in the untreated Ba/F3 cells. One sample t-tests are used for determining the statistical significance. (C) Comparisons of BafA1-mediated rescue of surface MPL in control (EV) vs. CRT_{Del52} cells. The p-value is calculated using a paired t-test analysis. Panels B and C include data from 12 experiments from 4 independent transductions of BaF3-MPL cells. **(D and E)** Ba/F3-MPL control (EV) and Ba/F3-MPL CRT_{Del52} cells were treated with inhibitors of proteasomal degradation, MG132 (D) or Bortezomib (E) at the indicated concentrations for 4h at 37 °C in media with IL-3. Surface MPL levels measured by flow cytometry are plotted as a ratio of MFI values in treated relative to untreated cells (n=3). **(F)** Representative blots (n=5) for MPL in the lysates of Ba/F3-MPL (EV), Ba/F3-MPL-CRT_{WT} or Ba/F3-MPL-CRT_{Del52} cells as indicated, treated with 21 µM MG132, 100 nM BafA1 or both. The immature form of MPL protein (I) and the two distinct mature forms, M1 (partially mature MPL expressed in CRT_{Del52} cells) and M2 (detected in CRT_{WT} expressing cells), are indicated within the MPL blot. Ubiquitin and p62 were probed as markers to show successful inhibition of proteasomal and lysosomal degradation, respectively. **(G)** Bar graphs show quantifications of total, immature and mature/partially mature MPL protein in Ba/F3-MPL CRT_{Del52} cells treated with MG132 and/or BafA1 normalized to the values on untreated cells based on immunoblots. Image J was used for quantification of blots. One sample t-tests are used to determine the statistical significance. Graphs were plotted using GraphPad Prism. EV, Empty Vector; IL-3, Interleukin 3; ns, non-significant

Figure 5: Inhibition of lysosomal degradation rescues CRT_{Del52} levels whereas the proteasomal pathway inhibition promotes CRT_{Del52} degradation. (A-D) Representative immunoblots (n=2) show CRT_{Del52} levels (A and C) in the lysates of control (EV) or CRT_{Del52} expressing Ba/F3-MPL cells treated for 4 h with different concentrations of MG132 (A) or Bortezomib (C). Bar graphs (B and D) show quantifications of CRT_{Del52} band intensities from blots of Ba/F3-MPL CRT_{Del52} cells (n=2) treated with different concentrations of MG132 (B) or Bortezomib (D) normalized to CRT_{Del52} band intensities in untreated cells. **(E)** Representative histograms of surface CRT detected by flow cytometry using mutant CRT-specific antibody (anti-CRT(C_{mut})) on Ba/F3-MPL, Ba/F3-CRT_{Del52} and Ba/F3-MPL CRT_{Del52} cells. **(F)** Bar graph shows MFI of surface CRT, detected by anti-CRT(C_{mut}) antibody on Ba/F3-MPL CRT_{Del52} cells treated with 21 µM MG132 and/or 100 nM BafA1 normalized to the MFI values for untreated cells (n=5). **(G-I)** Ba/F3-MPL, Ba/F3-CRT_{Del52} or Ba/F3-MPL CRT_{Del52} cells as indicated were treated with 21 µM MG132 or 100 nM BafA1 or both drugs for 4 h at 37ºC in media with IL-3. The representative blots (n=5) show levels of cellular CRT_{Del52} (G). Graphs show band intensities of CRT_{Del52} quantified from immunoblots of lysates of drug-treated Ba/F3-CRT_{Del52} or Ba/F3-MPL CRT_{Del52} cells normalized to band intensities of untreated cells (H) or paired comparisons of band intensities from MG132-treated cells relative to those in cells treated with MG132+BafA1 (I). **(J)** Representative blot of secreted CRT_{Del52} immunoprecipitated (IP) with anti-CRT(C_{mut}) antibody from cell culture media of Ba/F3-CRT_{Del52} cells (n=2) and Ba/F3-MPL CRT_{Del52} cells (n=6) that were either untreated or treated with 21 µM MG132 and/or 100 nM BafA1 for 4h at 37ºC in media with IL-3. **(K and L)** Quantification of secreted CRT_{Del52} band intensities from IP/immunoblots normalized to the values for untreated cells (K) and line graphs of CRT_{Del52} band intensities from MG132-treated cells relative to those in cells treated with MG132+BafA1 (L). Each line in graphs I and L represents an individual experiment and lines connect datapoints for the indicated treatments within experiments. CRT_{Del52} in A, C, G, and J were probed using anti-CRT(C_{mut}) antibody. GAPDH blots in panels A, C and G show equal loading of lysates in different lanes. Image J was used for quantification of blots. Graphs were plotted using GraphPad Prism. Statistical significance

was determined using one-sample t-tests in panels B, D, F, H and K and paired t-tests in panels I and L. p-values <0.05 are shown. ns, non-significant

Figure 6: Inhibition of lysosomal degradation promotes localization of MPL and CRT_{Del52} in LAMP1 compartments. HEK293T cells transfected to express human MPL along with either CRT_{WT} or CRT_{Del52} were either left untreated or treated with 100 nM BafA1 for 4h at 37°C, fixed and immunostained for LAMP1 (green), MPL (red) and either CRT_{WT} (anti-CRT(N)) or CRT_{Del52} (anti-CRT(C_{mut})) (blue) proteins. Nuclei were stained with DAPI. **(A)** Representative Airyscan microscopy images (n=2) showing a single z-slice of untreated and treated HEK293T cells expressing specific proteins and stained with specific antibodies as indicated. Zoomed view of the inset is shown and arrowheads point to the CRT_{Del52} and MPL puncta colocalizing within LAMP1 compartments. Scale bar is 5 µm in all the images except the zoomed inset images where scale bar is 2 µm **(B-F)** Graphs show quantification of CRT puncta (B), MPL puncta (C), fraction of MPL puncta colocalizing with CRT (D), fraction of CRT puncta colocalizing with LAMP1 structures (E) and fraction of LAMP1 structures colocalizing with CRT or MPL (F) in BafA1-treated cells expressing either CRT_{Del52} (82 cells from two experiments) or CRT_{WT} (91 cells from two experiments). Data were quantified using segmentation and analysis platform CellProfiler. Graphs were plotted using GraphPad Prism and statistical significance is determined using unpaired t-tests.

Figure 7: mTOR inhibitors reduce CRT_{Del52} mediated cytokine-independent proliferation and colony-forming capacity of $CD34^+$ cells from MPN patients. (A, C, E, G and I) Representative proliferation plots of Ba/F3-MPL (A, C and I) or Ba/F3-MPL-CRT_{Del52} (E and G) cells that are treated with or without 50 nM Rapamycin (A and E, n=3) or 100 nM Rapamycin (A and E, n=6; I, n=3), or 100 nM Everolimus (C, n=4; G, n=8 and I, n=3), either in the presence of IL-3 (A and C) or human TPO (I) or in the absence of any cytokine (cytokine-independent; E and G) as indicated. **(B, D, F, H and J)** Averaged relative proliferation corresponding to the conditions shown in A, C, E, G and I. Cell counts of the untreated cells were set at 100% for all the time points**.** Two-way ANOVA analyses (B, F and J) and multiple paired t-tests (D and H) were used to determine statistical significance (indicated by p-values) on different days. **(K and L)** Representative blots of lysates of Ba/F3-MPL CRT_{Del52} cells treated with 100 nM Rapamycin (K) or 100 nM Everolimus (L) that were harvested at different time points during proliferation assays and compared to the untreated cells. Two serial dilutions of each lysate were loaded in consecutive lanes as indicated. **(M)** Representative blot of secreted CRT_{Del52} immunoprecipitated (IP) using anti-CRT(C_{mut}) antibody from culture media of Ba/F3-MPL CRT_{Del52} cells (n=3) collected on different days of cytokine-independent proliferation assay with or without 100 nM Everolimus treatment. Lysates of untreated Ba/F3-MPL and Ba/F3-MPL CRT_{Del52} cells growing in the presence of IL-3 were loaded as controls in the specified lanes. CRT_{Del52} blots (K, L and M) and MPL blots (K and L) were probed with anti-CRT(C_{mut}) and anti-MPL antibodies, respectively. GAPDH blots (K and L) show relative loading of lysates as indicated. LC3 blots (K and L) show autophagy activation upon rapamycin or everolimus treatment as indicated by LC3-II bands (arrow). **(N-Q)** $CD34^+$ hematopoietic stem cells (HSCs) isolated from bone marrow samples of MPN patients or mobilized leukopaks from healthy donors were either plated on semi-solid methylcellulose containing media (N and O) or in liquid cultures containing StemSpan™ megakaryocyte expansion supplement (P and Q) with or without 50 nM (N and O) or 100 nM Everolimus (P and Q). $CD34^+$ cells were either treated with or without 50 nM Everolimus for 24h before plating (pre-treatment) (N) or everolimus was added into the plating media (continuous treatment) (O). The number of colonies were counted 12-18 days after plating either manually or using Image J. Each dot indicates an individual healthy donor (three healthy donors), or patient (six independent collections from 5 patients) and lines connect untreated and treated values for each donor/patient. Cells growing in the megakaryocyte expansion supplement were collected on Day 7 after seeding, stained for surface CD41 and CD42a markers and analyzed by flow cytometry. The gating strategy used for analysis of $CD41^+CD42a^+$ cells is shown (P). The percentage of $CD41^+CD42a^+$ cells under untreated and treated conditions measured on Day 7 are plotted (Q). Each dot indicates an individual healthy donor (seven independent experiments with four healthy donor samples), or patient (six patients) and lines connect untreated and treated values for each donor/patient. Statistical significance is calculated using paired t-tests and graphs were plotted using GraphPad Prism (N and P). All p-values ≤0.05 are shown.

Figure 1

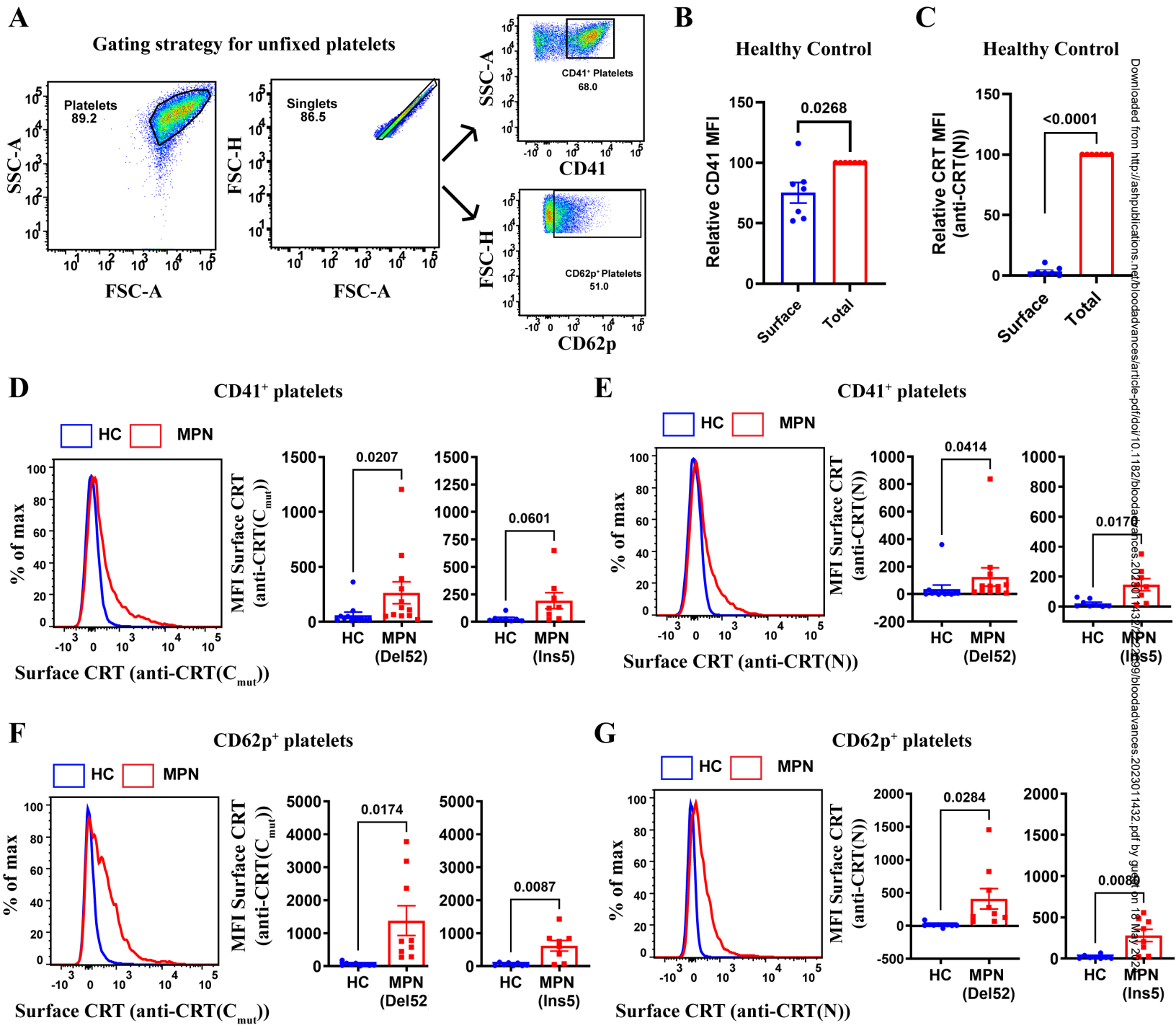

Figure 2

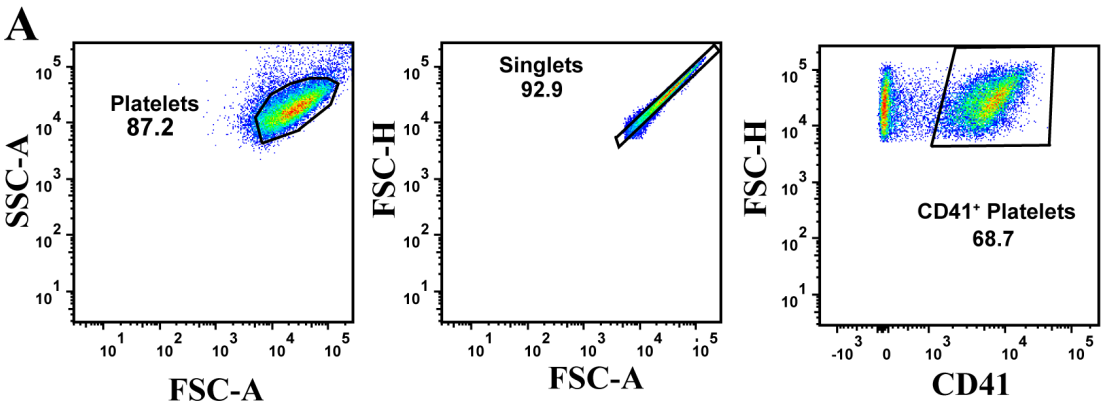

Gating strategy for
fixed and permeabilized platelets

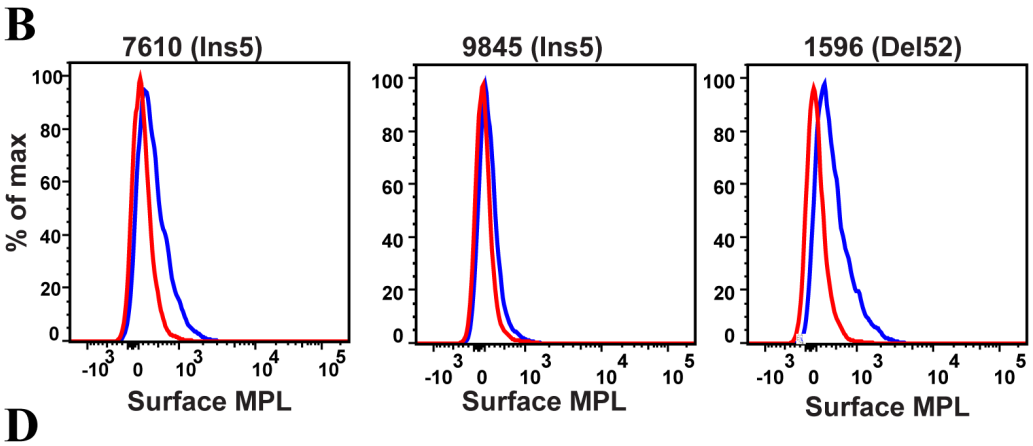

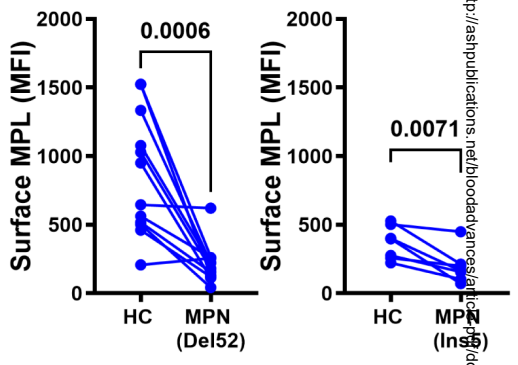

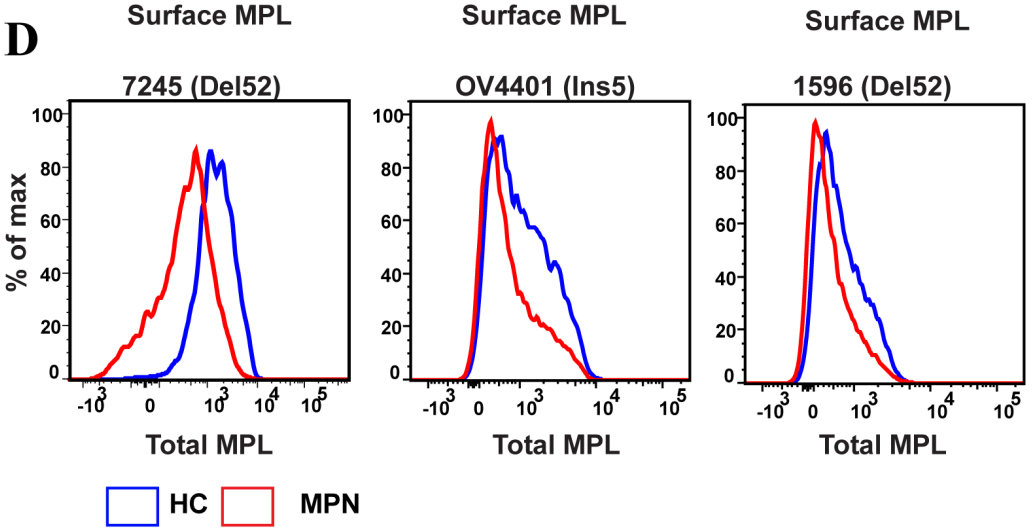

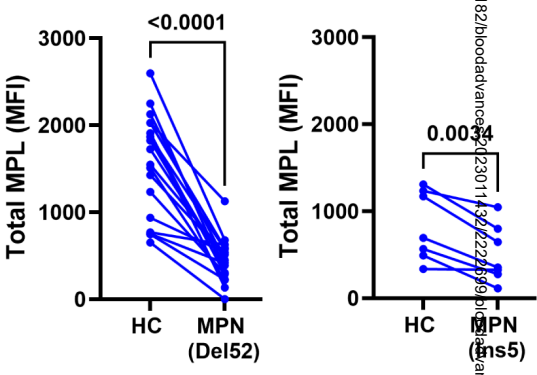

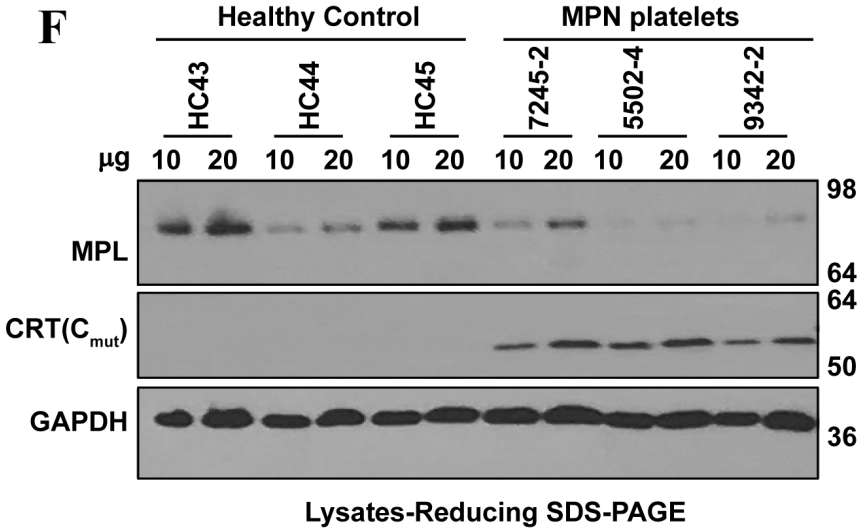

Figure 3

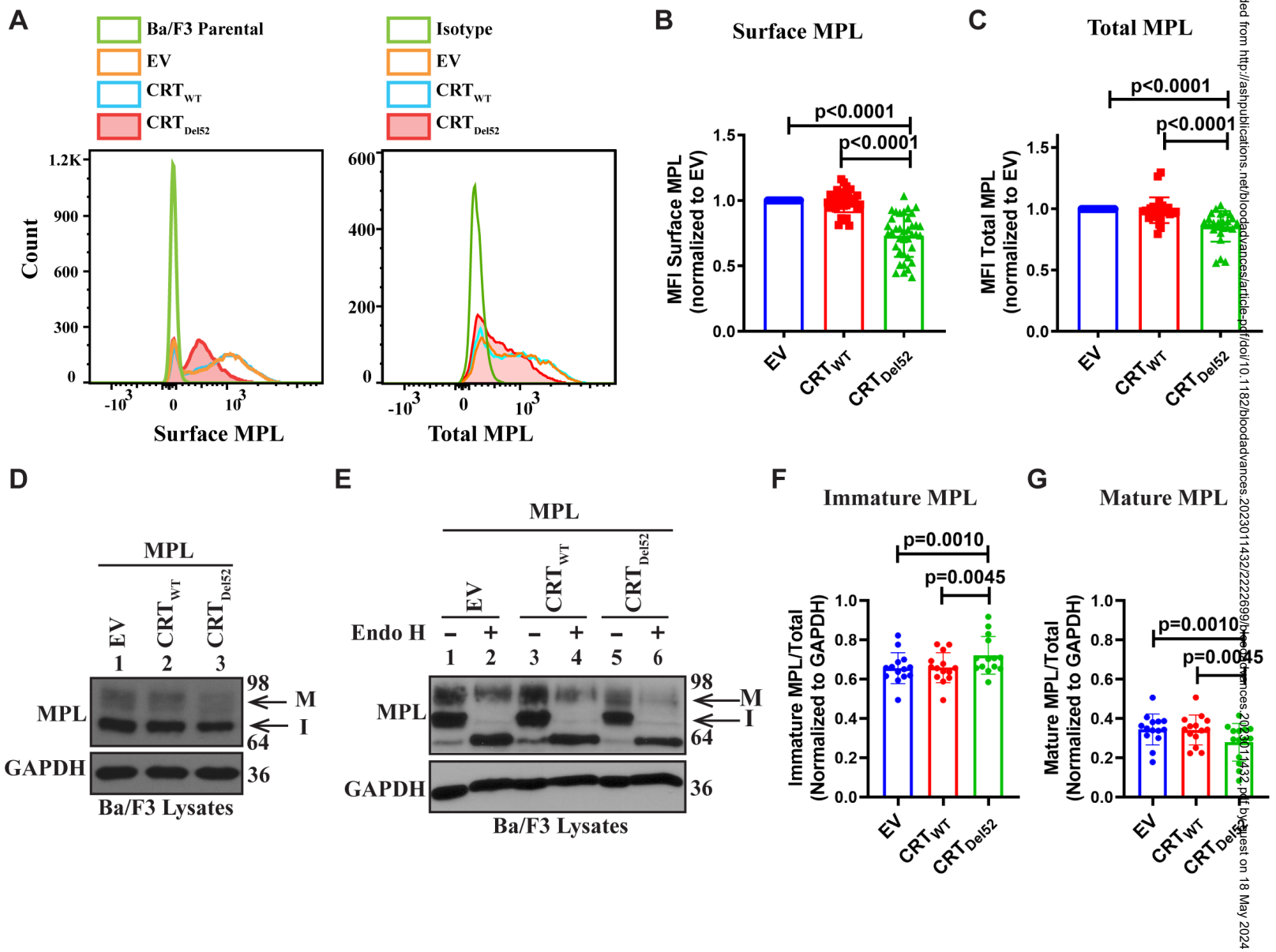

Figure 4

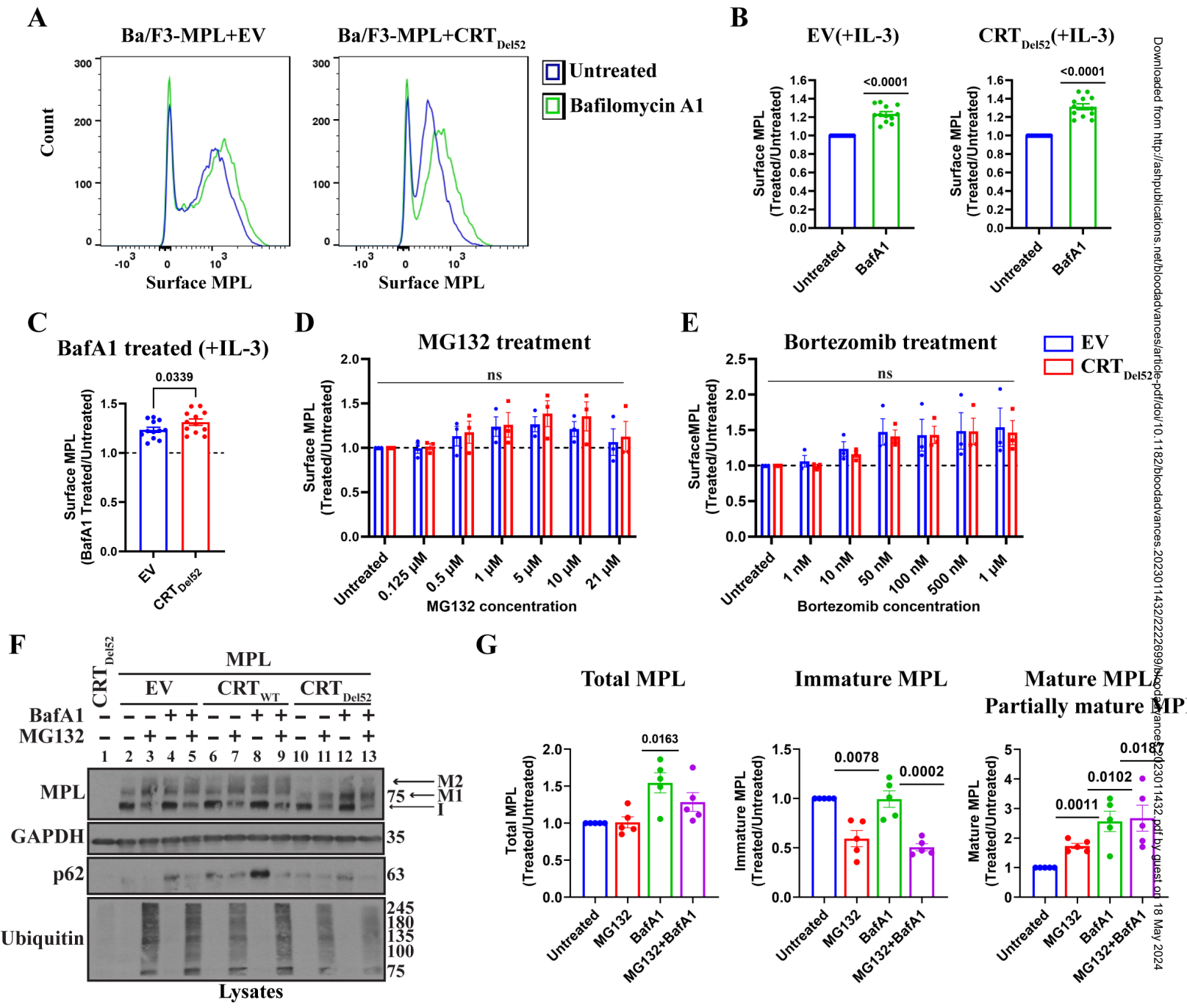

Figure 5

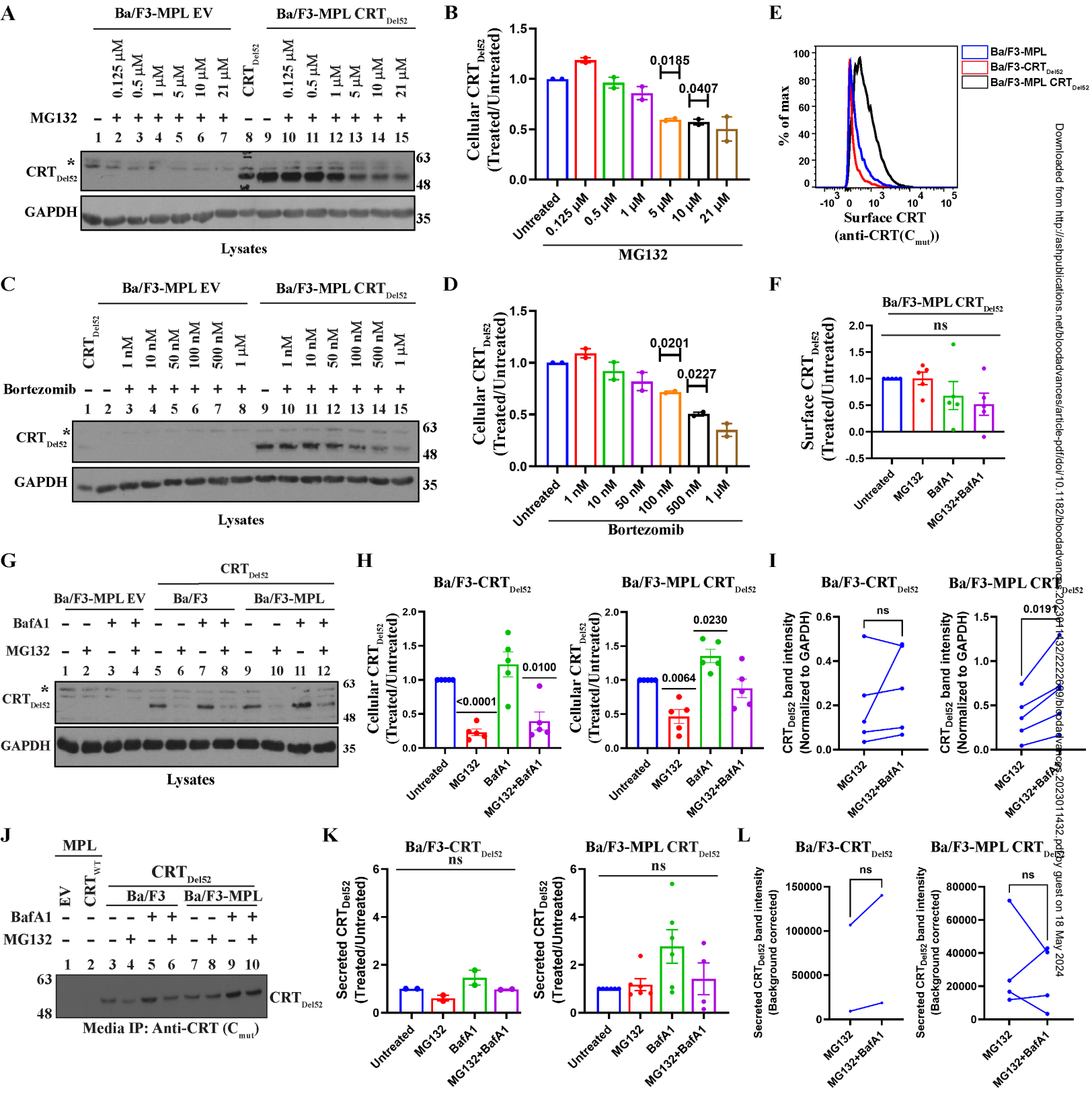

Figure 6

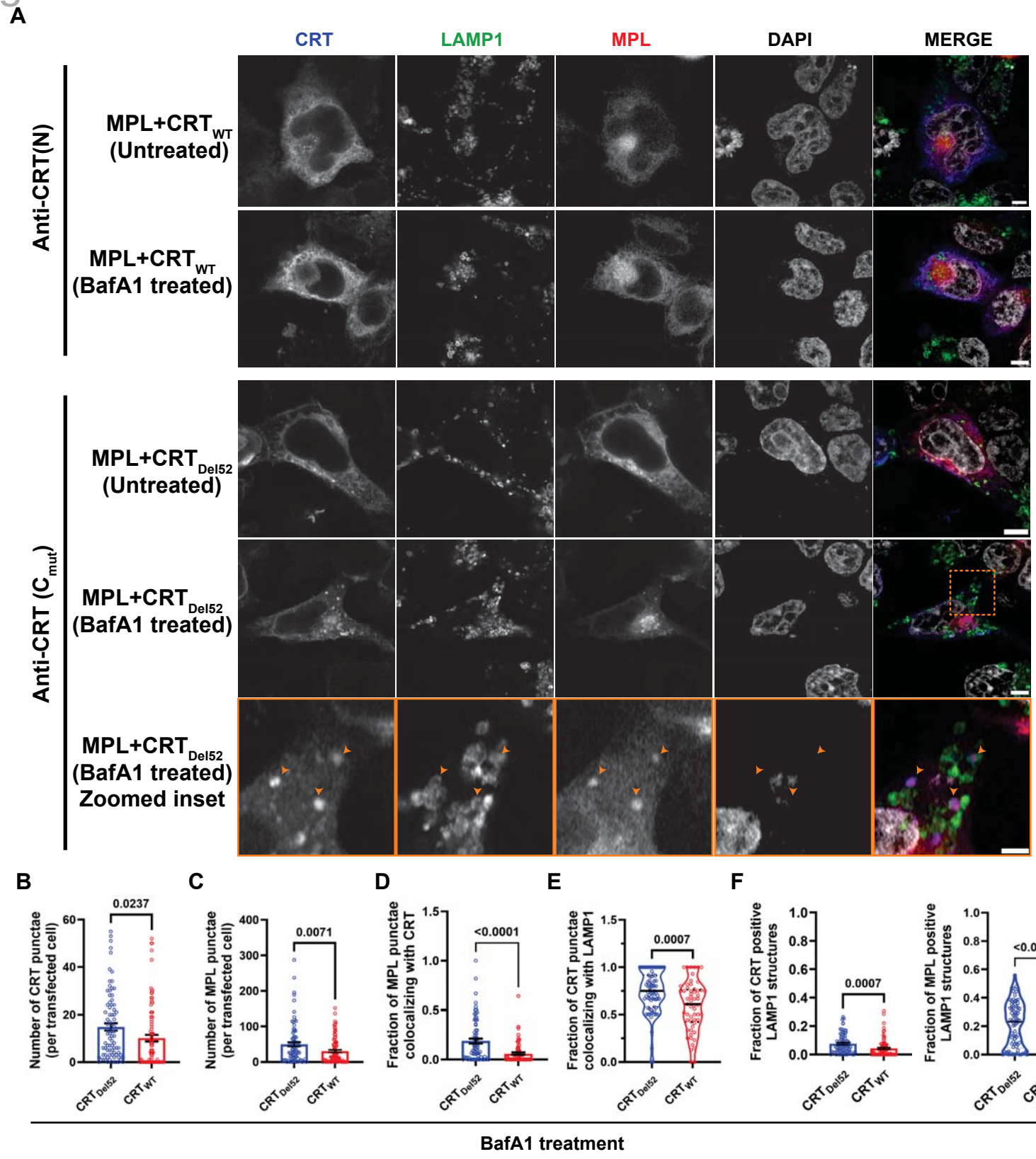

Figure 7